



An Analytical Modeling on Flow and Heat Transfer for a Pressure-Driven Electroosmotic Flow in Microchannel Considering First Order Slip Model

Avisankha Dutta¹ · Sudip Simlandi¹

Received: 26 August 2020 / Accepted: 2 April 2021 / Published online: 20 April 2021
© The Institution of Engineers (India) 2021

Abstract An analytical solution to study fundamental behaviors of a pressure-driven electroosmotic flow in a parallel plate microchannel is presented in the present work. A thermally fully developed flow of a Newtonian liquid is considered. The fluid motion is assumed to be caused with a pressure gradient applied externally and an electrostatic potential field. The electrical potential field is determined by solving the Poisson–Boltzmann equation. The Debye–Huckel approximation is not considered for higher accuracy of results. A modified form of the Navier–Stokes equation with slip boundary conditions is considered to evaluate velocity field and skin friction coefficient, whereas the energy equation is simplified to obtain temperature profile as well as Nusselt number. Homotopy perturbation method (HPM) is applied to solve the Poisson–Boltzmann equation, whereas the momentum and the energy equations has been solved analytically to achieve the velocity and temperature profiles, respectively. The predicted results are compared with existing work and show a good harmony. Results obtained for electric potential, velocity and temperature fields have been shown graphically varying wall zeta potential, slip coefficient and pressure gradient. Subsequently, a parametric study is presented for skin friction coefficient and the Nusselt number. Finally, an effort is made to determine local volumetric entropy generation and global entropy generation. The proposed results exhibit both the influence of the Brinkman number and pressure gradient on the entropy generation.

Keywords Microchannel · Parallel plates · Pressure-driven electroosmotic flow · Zeta potential · Nusselt number · Entropy generation

List of Symbols

$2H$	Distance between two parallel plates (m)
ψ	Electric potential due to EDL (V)
Ψ	Non-dimensional electric potential
Υ	Perpendicular distance of a given point from the center (m)
n_0	Bulk ionic concentration (m^{-3})
Z	Valence of ions
E	Electric charge (C)
k_b	Boltzmann constant (J K^{-1})
T	Absolute temperature (K)
ξ	Zeta potential at the wall (V)
Z	Non-dimensional zeta potential
κ	Inverse Debye–Huckel length (m^{-1})
λ	Electrokinetic length (m)
μ	Dynamic viscosity (Pa s)
U	Velocity in x -direction (m s^{-1})
u_m	Mean velocity (m s^{-1})
U	Non-dimensional velocity
F_x	Electrical force per unit volume of the liquid (N m^{-3})
E_x	Electric field strength (V m^{-1})
E	Non-dimensional electric field strength
β	Slip coefficient (m)
ρ_f	Local net charge density (cm^{-3})
L	Distance between the two electrodes (m)
$C_1, \Delta P$	Non-dimensional pressure gradient
C_2	Ratio of electrical force per unit volume to frictional force per unit volume
B	Slip coefficient

✉ Sudip Simlandi
sudip.simlandi@gmail.com

¹ Department of Mechanical Engineering, Jadavpur University, Kolkata 700032, India

q_w	Heat flux at wall (W m^{-2})
C_f	Skin friction coefficient
τ_w	Shear stress (MPa)
ρ	Density (kg m^{-3})
c_p	Specific heat ($\text{J kg}^{-1} \text{K}^{-1}$)
T_w	Wall temperature (K)
T_m	Mean temperature (K)
Φ	Non-dimensional temperature
θ	Non-dimensional temperature at wall
Nu	Nusselt number

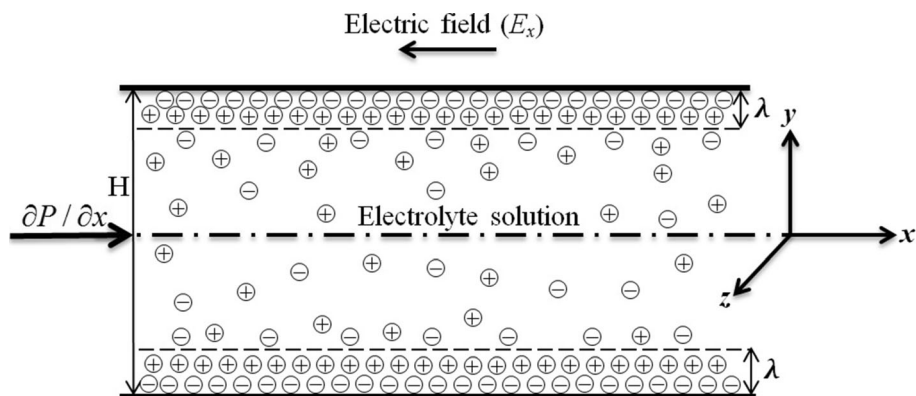
Introduction

In current years, microfluidic systems are rapidly becoming a significant area of study for numerous prospective applications in chemical and biomedical sectors. Microfluidic-based bioMEMS or lab-on-a-chip devices can execute sample separation, injection, chemical reaction and finding in an assimilated microfluidic circuit [1, 2]. The most important microfluidic operations in various bioMEMS are pumping, mixing, thermal cycling, dispensing and separating. Many methods like thermopneumatic, magnetohydrodynamic, electrostatic, piezoelectric and electroosmotic pumping are offered for fluid transport in microchannels [3–6]. The electroosmotic pumping is preferred among these methods due to simplicity of microfabrication and a great degree of flow regulation. Recently, electroosmotic pumps have been presented as a substitute to the porous media based electroosmotic pump. It is essential to gather knowledge on basic characteristics of EOF in microchannels for optimum design of electroosmotic pumps. The ions of an electrolyte solution dissociate when the solution is in no flow situation. These ions have charge reverse to that of the solid surface and have been invited by the solid surface. As a result, dual layers of positive and negative charged ions are built adjacent to the solid surface. These layers are termed electric double layer

(EDL) [7, 8]. When both electric field and pressure gradient is applied tangential to this charged solid surface, the ions from the diffuse layer start flowing due to a body force imposed by the electrical field, resulting a combined pressure-driven EOF [9]. EOF offers a very flat velocity profile. Moreover, switching without valves, precise regulator of conveyance and handling of liquid sample with an electrical field and absence of moving parts are few added advantages of electroosmotic pumping.

In this regard, some existing literatures are reviewed for a systematic idea on fluid delivery in microchannels. Burgreen and Nakache [10] investigated analytically electrokinetic liquid flow within a fine capillary channel of rectangular cross-section. The liquid transport is imposed by an electric field. The electrical potential distribution is determined considering the Debye–Huckel approximation. Masood Khan et al. [11] offer an exact analytical solution of a Burgers fluid in a cylindrical domain adopting temporal Fourier transform and Hankel transform. They considered a time periodic electroosmotic flow. It is finally concluded that the size of EDL thickness and velocity rises as the electrokinetic parameter is increased. Yang and Li [12] studied the influences of EDL adjacent to the two phase boundary and the imposed electro kinetic field of a pressure imposed flow in rectangular microchannels. An accurate solution of the momentum equation is determined adopting Green function formulation. They concluded that the liquid flow is influenced by the EDL field for high zeta potential. Jain and Jensen [13] established an analytical model to examine the influence of electrokinetics for fluid motion in microchannels. The momentum equation is modified assuming the Debye–Huckel linear approximation to determine velocity profile. The heat transfer analysis has also been studied. They concluded that the electrokinetic effects have considerable effect on fluid flow whereas the effect on heat transfer characteristics is negligible. Ngoma and Erchiqui [14] studied numerically the influence of slip factor and heat flux for pressure-driven EOF of liquid within parallel plate microchannel. They considered the Poisson–Boltzmann equation for electric

Fig. 1 Schematic of the physical problem



potential field, the reduced momentum equation for fluid flow behaviors and the energy equation for heat transfer characteristics. It is concluded that the slip factor, pressure gradient and heat flux influence the fluid motion and heat transfer in different manner. Shamshiri et al. [15] carried out the 1st and 2nd law analysis for electroosmotic pressure-driven flow of non-Newtonian liquid within uniform micro-annulus. They solved numerically the governing equations in cylindrical polar coordinates using finite difference method. In the second law analysis, the entropy generation rates are determined and the influence of thermal diffusion, Joule heating and viscous dissipation are examined on the total entropy generation. Wang and Jian [16] investigated the thermal transport characteristics of fluid in slit nanochannels under the joint influences of streaming potential and pressure driven. The non-dimensional temperature distribution is analytically determined from the energy equation based on the obtained electric potential and velocity profiles. Finally, the entropy generation rates are obtained and presented graphically.

In general, the electric potential field for electroosmotic flow in microchannels is obtained using a simple analysis implementing the Debye–Hückel approximation. The approximation is effective only if the wall zeta potential is very small [14, 17–20]. However, higher orders of zeta potential are often faced in real-life applications. Hence, the accuracy of predicted result becomes less. For such instances, in place of the Debye–Hückel approximation tedious and time-consuming numerical simulations are used. Alternatively, the analytical techniques used in the literature are lengthy, laborious and complex. Therefore, it becomes very essential to apply a simple analytical technique to predict the essential behavior of EOF in microchannels disregarding the Debye–Hückel approximation.

This work considers a pressure-driven EOF within a parallel plate microchannel. The analytical technique HPM is used to determine solution of the Poisson–Boltzmann equation as an effective and a simple analytical solution technique. Subsequently, the electric potential distribution is utilized to solve the momentum equation for obtaining velocity distribution and the energy equation for determination of temperature profile.

Description of Physical Problem

Figure 1 shows liquid motion within a microchannel between two parallel plates. The plates are considered with a distance of H and assumed to be extended to both infinite x - and z -axis. Hence, variations of properties are assumed in the y -direction. Electrodes are positioned at a distance of L perpendicular to the plates so that an electric field (E_x) is

formed along x -axis. A fixed pressure gradient is applied along x -axis to investigate the mutual influence of both the pressure and electric fields.

The assumptions made in the analysis are as follows:

- The fluid is a Newtonian, incompressible and symmetric electrolyte.
- The thermophysical properties of the liquid are constant.
- A laminar, steady and fully developed flow is considered.
- First-order slip velocity boundary condition is considered.

Mathematical Formulation

The liquid flow based on the above assumptions is governed by the Poisson–Boltzmann, the reduced Navier–Stokes and the energy equations.

The Poisson–Boltzmann Equation

The differential equation for the EDL field in y -direction is presented by the Poisson–Boltzmann equation as [13, 17–19, 21, 22]

$$\partial^2\psi/\partial y^2 = (2ze\eta_0/\epsilon) \sinh(ze\psi/k_bT) \tag{1}$$

The boundary conditions of Eq. (1) stated as follows:

For $y = H/2$, $\partial\psi/\partial y = 0$ and for $y = 0$, and at H , $\psi = \zeta$.

Momentum Equation

The modified Navier–Stokes equation in x -direction is given by a equilibrium among the electric field, externally applied pressure gradient and shear stresses as [13, 14]

$$\mu(\partial^2u/\partial y^2) - \partial P/\partial x + F_x = 0 \tag{2}$$

, where $F_x = \rho_f E_x$ denotes electrical force of the liquid/unit volume.

Therefore, Eq. (2) becomes

$$\mu(\partial^2u/\partial y^2) - \partial P/\partial x + \rho_f E_x = 0 \tag{3}$$

The boundary conditions of Eq. (3) are

For $y = 0$, $u = \beta(\partial u/\partial y|_{y=0})$ whereas for $y = H$, $u = -\beta(\partial u/\partial y|_{y=H})$.

Energy Equation

The energy equation of a laminar steady thermally fully developed flow is written as [13, 14]

$$\rho C_p u (\partial T/\partial x) = k(\partial^2 T/\partial y^2) + E_x^2 \sigma \tag{4}$$

The boundary conditions of Eq. (4) are

For $y = 0$, $-k(\partial T/\partial y) = q_w, T = T_w$ and at $y = H$, $k(\partial T/\partial y) = q_w, T = T_w$.

Solution Method

The governing equation for the electrical potential has been solved adopting HPM. Subsequently, the velocity and temperature distributions are obtained analytically based on the obtained electrical potential field.

Electric Potential Field

Solving Eq. (1) adopting the HPM, the electric potential field is obtained. The following non-dimensional variables are introduced to dimensionless Eq. (1) as

$$\Upsilon = y/H, \Psi = ze\psi/(k_b T), Z = 2ze\xi/(k_b T)$$

Equation (1) is written in dimensionless form as

$$\partial^2 \Psi / \partial \Upsilon^2 = \lambda^2 \sinh \Psi \tag{5}$$

, where $\lambda = \kappa H$ and $\kappa = \sqrt{[2z^2 e^2 n_0 / (\epsilon k_b T)]}$.

The non-dimensional form of the corresponding boundary conditions are given as at $\Upsilon = 1/2$, $\partial \Psi / \partial \Upsilon = 0$ and at $\Upsilon = 0$ and at $\Upsilon = 1$, $\Psi = Z$.

It is already stated that most of the literature studied considers the Debye–Huckel approximation in which $\sinh \Psi$ of Eq. (5) is assumed as Ψ . Hence, accurateness of results might be reduced. The Debye–Huckel approximation in the current study is not assumed to increase the accurateness of the predicted results. Hence, $\sinh \Psi$ in Eq. (5) is taken as $\sinh \Psi$ which is expressed following the Taylor’s expansion series.

$$\sinh \Psi = \Psi + \Psi^3/3! + \dots \tag{6}$$

Putting Eq. (6) in Eq. (5) leads to

$$\partial^2 \Psi / \partial \Upsilon^2 = \lambda^2 (\Psi + \Psi^3/3! + \dots) \tag{7}$$

A homotopy is constructed to solve Eq. (5) as

$$\Psi'' - \omega^2 \Psi + p [(\lambda^2 - \omega^2) \Psi + \lambda^2 \Psi^2/3] = 0 \tag{8}$$

, where $\Psi'' = \partial^2 \Psi / \partial \Upsilon^2$, ω denotes a reformed inverse Debye length. Whereas $p \in [0, 1][0, 1]$ signifies a trivial term called embedding parameter in the HPM based analysis.

The electrical potential Ψ is expressed with a power series in p as

$$\Psi = \Psi_0 + p \Psi_1 + p^2 \Psi_2 + \dots \tag{9}$$

Substituting Eqs. (9) to (8) and ordering the constants of p powers, the equation can be expressed as follows

$$p^0 (\Psi_0'' - \omega^2 \Psi_0) + p^1 [\Psi_1'' - \omega^2 \Psi_1 - (\lambda^2 - \omega^2) \Psi_0 - \lambda^2 \Psi_0^3/3!] = 0 \tag{10}$$

Equating the coefficients of p^0, p^1 to zero provides

$$p^0 : \Psi_0'' - \omega^2 \Psi_0 = 0 \tag{11}$$

$$p^1 : \Psi_1'' - \omega^2 \Psi_1 - (\lambda^2 - \omega^2) \Psi_0 - \lambda^2 \Psi_0^3/3! = 0 \tag{12}$$

Equation (11) is solved using the boundary conditions $\Psi_0(0) = Z, \Psi_0(1) = Z$ and $\Psi_0'(1/2) = 0$ resulting in

$$\Psi_0 = Z \cosh\{\omega(\Upsilon - 1/2)\} / \cosh(\omega/2) \tag{13}$$

Replacing Eq. (13) in Eq. (12) and simplifying the equation gives

$$\Psi_1'' - \omega^2 \Psi_1 - (\lambda^2 - \omega^2) Z \cosh\{\omega(\Upsilon - 0.5)\} / \cosh(\omega/2) - \lambda^2 Z^3 [3 \cosh\{\omega(\Upsilon - 1/2)\} + \cosh\{3\omega(\Upsilon - 1/2)\}] / [24 \cosh^3(\omega/2)] = 0 \tag{14}$$

In order to eliminate $\cosh\{\omega(\Upsilon - 0.5)\}$ in Eq. (14), the coefficients are collected and equated to zero as

$$(\lambda^2 - \omega^2) Z / \cosh(\omega/2) + \lambda^2 Z^3 / [8 \cosh^3(\omega/2)] = 0$$

to give the value of ω as follows

$$\omega = \sqrt{[(8\lambda^2 - 8) + \sqrt{(\lambda^2 + 4)^2 + 2z^2}]/2} \tag{15}$$

Equation (14) becomes

$$\Psi_1'' - \omega^2 \Psi_1 - \lambda^2 Z^3 \cosh\{3\omega(\Upsilon - 1/2)\} / [24 \cosh^3(\omega/2)] = 0 \tag{16}$$

Now applying the boundary conditions.

$$\Psi_1(0) = 0, \Psi_1(1) = 0 \text{ and } \Psi_1'(1/2) = 0.$$

Equation (16) is solved and written as

$$\Psi_1 = [\lambda^2 Z^3 / 192 \omega^2 \cosh^3(\omega/2)] [\cosh\{3\omega(\Upsilon - 1/2)\} + \cosh(3\omega/2) \cosh\{\omega(\Upsilon - 1/2)\} / \cosh(\omega/2)] \tag{17}$$

Replacing Eqs. (13) and (17) in Eq. (9) and taking $p = 1$, the electric potential field is evaluated as

$$\Psi = A_1 \cosh\{\omega(\Upsilon - 1/2)\} + A_2 \cosh\{3\omega(\Upsilon - 1/2)\} \tag{18}$$

$$\text{where } A_1 = Z / \cosh(\omega/2) - \lambda^2 Z^3 \cosh(3\omega/2) / [192 \omega^2 \cosh^4(\omega/2)] \text{ and } A_2 = \lambda^2 Z^3 / [192 \omega^2 \cosh^3(\omega/2)].$$

Velocity Field

The modified momentum equation is written as [19]

$$\mu(\partial^2 u/\partial y^2) = \partial P/\partial x + \varepsilon E_x \partial^2 \psi/\partial y^2 \tag{19}$$

, where $\rho_f = -\varepsilon(\partial^2 \psi/\partial y^2)$ is the local net charge density.

The following dimensionless terms are introduced to non-dimensionalized Eq. (19) as

$$U = u/u_m, C_1 = -(H^2/\mu u_m)\partial P/\partial x = \Delta P, \\ C_2 = \varepsilon k_b T E_x / (\mu u_m z e) \text{ and } B = u_m \beta / H$$

Hence, dimensionless form of Eq. (19) becomes

$$\partial^2 U/\partial Y^2 = -C_1 + C_2(\partial^2 \Psi/\partial Y^2) \tag{20}$$

Now, Eq. (20) is integrated twice with respect to Y yields

$$U = -C_1 Y^2/2 + C_2 \Psi + a_1 Y + a_2 \tag{21}$$

, where a_1 and a_2 are integration constants. The corresponding boundary conditions are presented in non-dimensional form as follows:

$$\text{at } Y = 0, U = B(\partial U/\partial Y|_{Y=0}) \text{ and at } Y = 1, \\ U = -B(\partial U/\partial Y|_{Y=1}).$$

Applying the above boundary conditions two linear equations are obtained as follows

$$-Ba_1 + a_2 = -C_2\{\Psi(0) + B\Psi'(0)\} = C_3 \tag{22}$$

$$(1 + B)a_1 + a_2 = C_1(B + 1/2) - C_2\{\Psi(1) + B\Psi'(1)\} \\ = C_4 \tag{23}$$

Solving Eqs. (22) and (23) the expressions for a_1 and a_2 are determined as follows:

$$a_1 = (C_4 - C_3)/(1 + 2B) \tag{24}$$

$$a_2 = \{(1 + B)C_3 + BC_4\}/(1 + 2B) \tag{25}$$

The skin friction coefficient C_f expressed as [13]

$$C_f = 2\tau_w/(\rho U^2) \tag{26}$$

The product $C_f Re$ determined as

$$C_f Re = 4U'(1) \tag{27}$$

, where $Re = \rho u_m (2H)/\mu$ is the Reynolds number.

Temperature Distribution

Equation (4) for an applied constant heat flux boundary condition results in where

$$\partial T/\partial x = \partial T_m/\partial x = \text{constant}$$

$$T_m = \int_0^1 UT dY \tag{28}$$

The energy balance for fluid flowing through a microchannel is written as follows:

$$\rho C_p u_m \partial T_m/\partial x = 2q_w/H + E_x^2 \sigma \tag{29}$$

Substituting Eq. (29) in Eq. (4) yields

$$u(2q_w/H + E_x^2 \sigma)/u_m = k(\partial^2 T/\partial y^2) + E_x^2 \sigma \tag{30}$$

Equation (30) is written in dimensionless form using the non-dimensional terms as follows:

$$\Phi = (T - T_m)/(Hq_w/k), H_1 = 2q_w/H + E_x^2 \sigma, \\ q_v = E_x^2 \sigma H/q_w \text{ and } \Phi_w = (T_w - T_m)/(Hq_w/k)$$

Hence, the non-dimensionalized energy equation becomes

$$\Phi = H_1 U - q_v \tag{31}$$

The non-dimensionalized boundary conditions are as follows:

$$\text{at } Y = 0, \partial \Phi/\partial Y = -1, \Phi = \Phi_w \text{ and at } Y = 1, \\ \partial \Phi/\partial Y = 1, \Phi = \Phi_w.$$

Equation (31) is integrated two times with respect to Y subjected to the above boundary conditions provides

$$\Phi_w - \Phi = H_1 C_1 (Y^4 - Y)/24 + H_1 C_2 [A_1 \{\cosh(\omega/2) \\ - \cosh \omega(Y - 1/2)\}/\omega^2 + A_2 \{\cosh(3\omega/2)\}/9\omega^2 \\ - \cosh 3\omega(Y - 1/2)] + H_1 a_1 (Y - Y^3)/6 \\ + H_1 a_2 (Y - Y^2)/2 + H_1 q_v (Y^2 - Y)/2 \tag{32}$$

The Nusselt number at the top and bottom plates expressed as [14]

$$Nu = q_w H / \{k(T_w - T_m)\} = 1/(\Phi_w - \Phi_m) \tag{33}$$

, where

$$\Phi_w - \Phi_m = \int_0^1 U(\Phi_w - \Phi) dY \tag{34}$$

Entropy Generation Rate

It is known from the 2nd law analysis of thermodynamics that the lost work is proportionate to the total entropy generation rate. Engineering devices and their components are to be operated at minimum destruction of work. As a result, minimization of entropy generation plays an important role in systematic design of these systems and components. It minimizes irreversibility existing in the real systems and processes. Hence, in this section, an effort is made to determine the local entropy generation rate as [15, 16]

$$S_G = S_{GH} + S_{GJ} + S_{GV} \tag{35}$$

, where S_{GH} , S_{GJ} and S_{GV} are the rate of local volumetric entropy generations resulting from heat diffusion, Joule heating and viscous dissipation, respectively, as described below

$$S_{GH} = k(\partial T/\partial y)^2/T^2 \tag{36}$$

$$S_{GJ} = \sigma E_x^2/T \tag{37}$$

$$S_{GV} = \mu(\partial U/\partial y)^2/T \tag{38}$$

S_G becomes dimensionless by introducing the following dimensionless terms

$$S_H = (\partial\Phi/\partial Y)^2/(\Phi + \theta)^2 \tag{39}$$

$$S_J = q_v/(\Phi + \theta) \tag{40}$$

$$S_V = Br(\partial U/\partial Y)^2/(\Phi + \theta) \tag{41}$$

, where $\theta = kT_w/(Hq_w)$ and $Br = \mu u_m^2/(Hq_w)$ is the Brinkmann number.

The non-dimensional global entropy generation rate is expressed as [15, 16]

$$S_{total} = \int_0^{1/2} (S_H + S_J + S_V)dY \tag{42}$$

Results and Discussion

This work considers an electroosmotic pressure-driven flow in a parallel plate microchannel with first order slip model. The electric potential, velocity, temperature profiles, the Nusselt number and the entropy generation rates are determined. Lastly, a MATLAB-based program is constructed for solving the constitutive governing equations. The results found are expressed in a comparative manner with both existing and numerical results for comparing accuracy level of the present study.

Effect of Zeta Potential on Electrical Potential Field

In Fig. 2, the non-dimensional potential distributions (Ψ) in the direction normal to the parallel plates (Y direction) are presented at $Z = 1, 2$ and 4 for an electrokinetic length (λ) of 10. It is observed that Ψ value increases from the center of the microchannel and reaches maximum value at

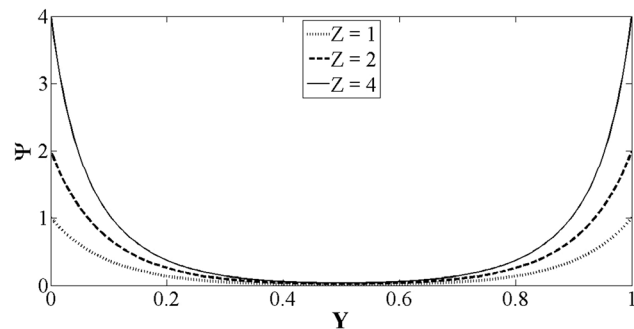


Fig. 2 Potential distribution for different values of zeta potential ($\lambda = 10$)

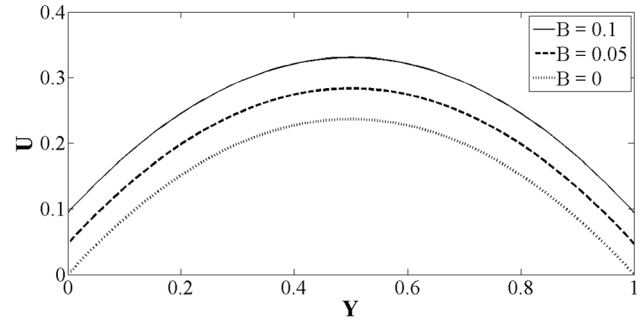


Fig. 3 Velocity profiles for different value of slip coefficient ($\lambda = 10, Z = 1, \Delta P = 1.9$)

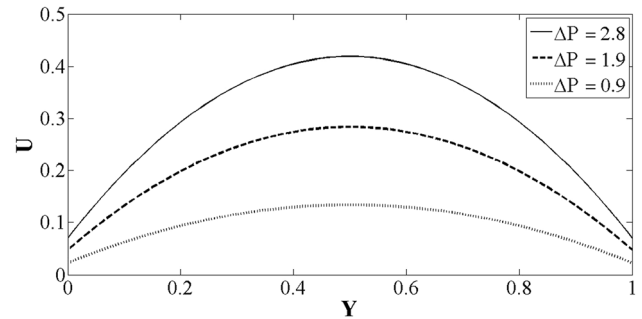


Fig. 4 Velocity profile for different pressure gradients ($\lambda = 10, Z = 1, B = 0.05$)

the walls. Moreover, the value of Ψ increases with increase in Z .

Effect on the Flow Velocity Profile

In Fig. 3, the non-dimensional velocity distribution (U) is presented with Y at $B = 0, 0.05$ and 0.1 for $\lambda = 10, Z = 1$ and $\Delta P = 1.9$. The velocity distribution for $B = 0$ corresponds to a familiar velocity profile with no slip boundary condition whereas the other profiles show velocity distribution with slip effect. The velocity profiles for $B = 0.05$ and 0.1 clearly depict that the increase in B leads to higher values of U . Hence, intensification in slip coefficient results in higher non-dimensional velocity of flow.

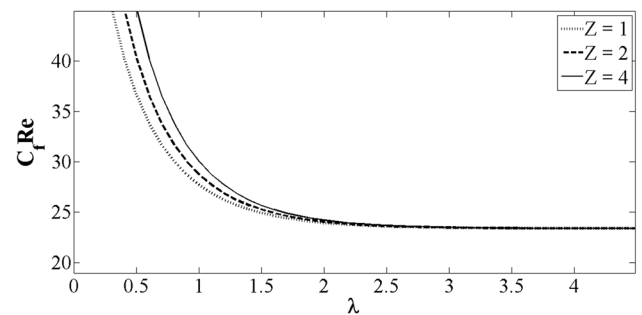


Fig.5 Nature of $C_f Re$ parameter for $Z = 1, 2, 3$ with λ

The influence of pressure difference on the velocity is shown in Fig. 4. The dimensionless pressure difference considered are $\Delta P = 0.9, 1.9$ and 2.8 for a constant non-dimensional slip coefficient of $B = 0.05$. It is observed that U rises as ΔP is raised. The rate of rise of U is higher as the ΔP value increases. It is noted that the curve for $\Delta P = 0.9$ is comparatively flat.

Influence of Wall Zeta Potential on the Product $C_f Re$

In Fig. 5, the $C_f Re$ product is expressed as a function of λ for $Z = 1, 2$ and 3 . It is noticed that the $C_f Re$ value decreases with increasing λ for a specific value of Z . With increase in λ , EDL field increases resulting an increase of C_f . At the same time, viscosity increases resulting an decrease in Re . But, the rate of decrease of Re is much faster than the rate of increase of C_f . As a result, $C_f Re$ product decreases as λ is increased. It is also noticed that for a specific λ value, the product $C_f Re$ rises with rise in Z . It might be explained as on increasing Z , the existence of EDL is noticed in a zone away from the solid wall resulting increase in viscosity which in turn enhances $C_f Re$ value.

Influence of Slip Coefficient and Pressure Gradient on Temperature Profile

To forecast the influence of slip coefficient on temperature difference, the non-dimensional pressure difference is kept constant ($\Delta P = 1.9$) as shown in Fig. 6. The slip coefficients chosen are $0.0, 0.05$ and 0.1 . It can be noticed that the temperature difference falls with rise in the slip coefficient. With increase in slip coefficient, the liquid flow velocity increases which in turn increases the convection heat transfer. In Fig. 7, the non-dimensional pressure difference ΔP is varied ($0.9, 1.9, 2.8$) for a constant non-dimensional slip coefficient (B) of 0.05 . It is noticed that the temperature rises with rise in ΔP for a specific location of Y .

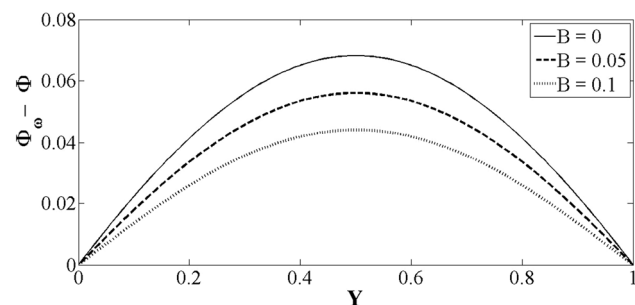


Fig. 6 Temperature distribution for different slip coefficients ($\lambda = 10, Z = 1, \Delta P = 1.9$)

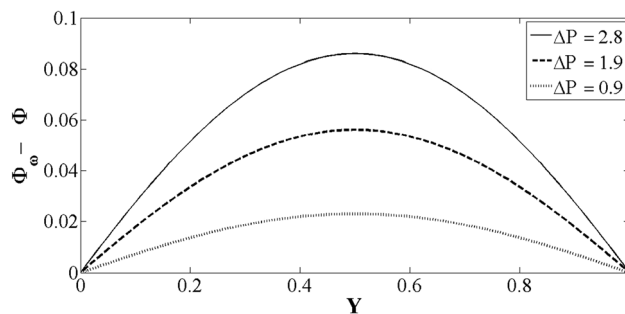


Fig. 7 Temperature profiles for different pressure gradient ($\lambda = 10, Z = 1, B = 0.05$)

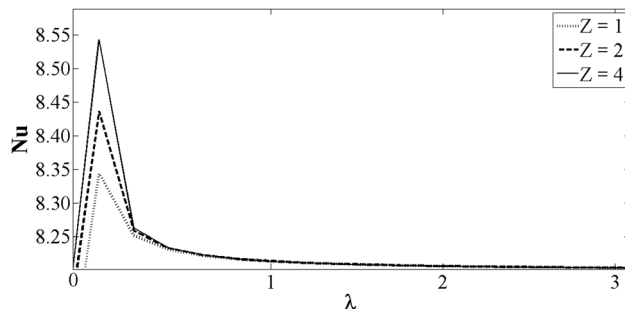


Fig. 8 Variation of Nu with λ for different values of Z ($\Delta P = 1.9, B = 0.05$)

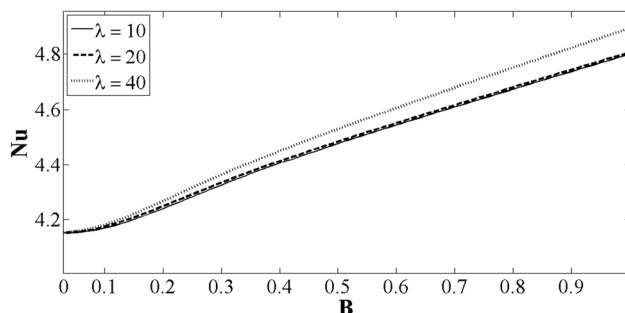


Fig. 9 Variation of Nu with B for different values of λ ($Z = 1, \Delta P = 1.9$)

Effect of Wall Zeta Potential and Electrokinetic Length on Nusselt Number

In this part, the effect of various flow parameters on Nu is studied. Figure 8 presents the variation of Nu with λ for $Z = 1, 2$ and 3 considering $\Delta P = 1.9, B = 0.05$. It is seen that Nu first increases, attains a peak value and then decreases. This may be explained as the creation of small turbulences in the flow field due to ionic distribution for smaller value of λ . Whereas for a larger value of λ , the wall is completely surrounded by counter-ions which in turns reduces the disturbances in the flow causing Nu to decrease with λ . It is also noticed from the same figure that for a particular value of λ , Nu increases as Z is increased. The electrostatic potential adjacent to the wall dominates more

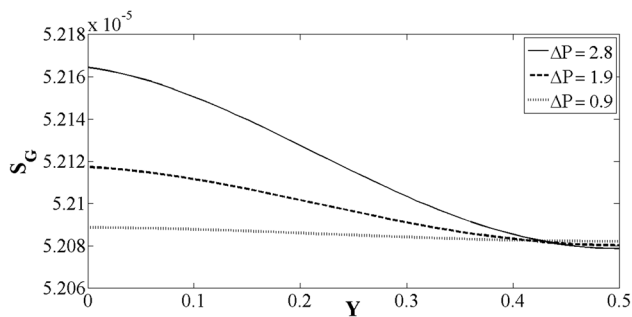


Fig. 10 Nature of S_G with Y for various pressure gradients ($\lambda = 10$, $Z = 1$, $B = 0.05$, $Br = 0.02$ and $\theta = 1000$)

with increase in Z resulting an increase in the apparent viscosity which causes Nu to increase.

In Fig. 9, Nu as function of dimensionless slip coefficient (B) is presented for changed values of electrokinetic length ($\lambda = 10, 20$ and 40) for a constant zeta potential (Z) and pressure difference (ΔP) of 1.0 and 1.9, respectively. It is seen that Nu rises with increasing B . An increase in B increases flow velocity U which in turn enhances the heat transfer coefficient resulting an increase in Nu .

Effect of Pressure Gradient on the Entropy Generation

This section deals with the influence of ΔP and Br on entropy generation rates. Figure 10 shows the variation of S_G with Y for $\Delta P = 0.9, 1.9$ and 2.8 considering $\lambda = 10$, $Z = 1$, $B = 0.05$, $Br = 0.02$ and $\theta = 1000$. It is observed that S_G rises from the center of the microchannel and becomes maximum at the wall. It is also noticed that S_G value increases with increasing ΔP upto a certain value of Y ($Y = 0.42$). This is due to the effect of electrical potential which is predominant adjacent to the wall and diminishes near the center. A part of the work associated with fluid delivery and heat transfer is lost in the process of electroosmotic flow, whose value is proportional to that of

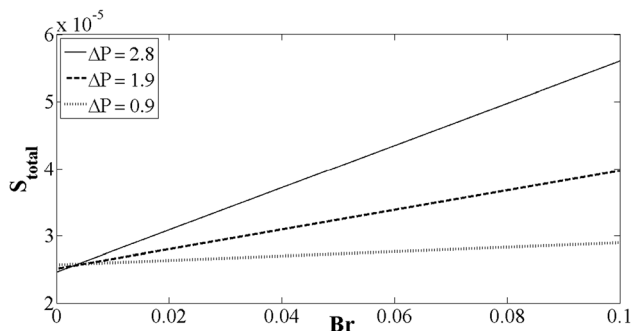


Fig. 11 Nature of S_{total} with Br for different pressure gradients ($\lambda = 10$, $Z = 1$, $B = 0.05$ and $\theta = 1000$)

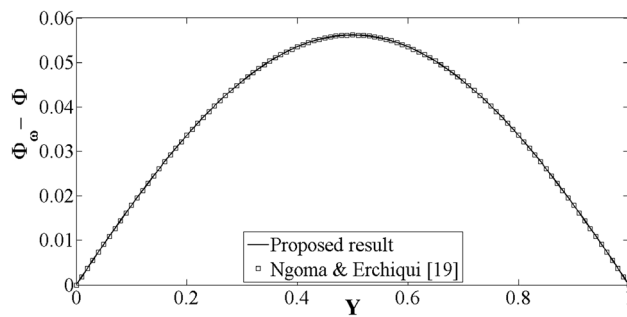


Fig. 12 Temperature distribution with Y ($\lambda = 10$, $Z = 1$, $\Delta P = 1.9$ and $B = 0.05$)

S_G . The lost work increases with increase in ΔP resulting an increase in S_G .

In Fig. 11, S_{total} is presented with Br for $\Delta P = 0.9, 1.9$ and 2.8 . It is seen that S_{total} increases with increasing both ΔP and Br . The influence of viscous dissipation rises with increase in Br , resulting an increased value of S_{total} . Moreover, with rise in ΔP , U increases causing S_{total} to increase.

Validation of the Present Work

The present analytical model is validated with the existing work by Ngoma and Erchiqui [14]. Figure 12 represents the temperature distribution based on present work with the Ngoma and Erchiqui [14] as a function of Y for $\lambda = 10$, $Z = 1$, $\Delta P = 1.9$ and $B = 0.05$. It is observed that the proposed result agrees well with the Ngoma and Erchiqui [14]. Therefore, the present analysis can be extended for analysis of pressure-driven electroosmotic flow between two plates.

Conclusion

This work proposes an analytical solution using HPM to investigate the behaviors of a pressure-driven electroosmotic flow considering first order slip model in a microchannel between two parallel plates. The electrical potential field is determined solving the Poisson–Boltzmann equation. The Debye–Huckel approximation is disregarded to recover accuracy of the proposed work. The velocity as well as temperature profiles are obtained solving the momentum and energy equations, respectively. The HPM is applied for solution of the constitutive governing equations. The potential distribution obtained is subsequently used to evaluate the velocity and temperature distributions. C_f and Nu are determined based on the velocity as well as temperature profiles. Both $C_f Re$ product and Nu increase with increase in zeta potential. Entropy generation rate is also evaluated. It is seen that entropy generation rises with increasing both pressure gradient and

Brinkman number. Finally, the proposed result is matched with existing work and shows a good harmony.

References

1. J. Coffel, E. Nuxoll, BioMEMS for biosensors and closed-loop drug delivery. *Int. J. Pharm.* **544**(2), 335–349 (2018)
2. B. Lin, A. Levchenko, Microfluidic technologies for studying synthetic circuits. *Curr. Opin. Chem. Biol.* **16**(3–4), 307–317 (2012)
3. C.G. Cooney, B.C. Towe, A thermopneumatic dispensing micropump. *Sens. Actuators* **116**, 519–524 (2004)
4. M. Kabir et al., Piezoelectric MEMS acoustic emission sensors. *Sens. Actuators B* **279**, 53–64 (2018)
5. Z.Y. Xie et al., Thermal transport of magnetohydrodynamic electroosmotic flow in circular cylindrical microchannels. *Int. J. Heat Mass Transf.* **119**, 355–364 (2018)
6. J.Y. Min et al., A novel approach to analysis of electroosmotic pumping through rectangular-shaped microchannels. *Sens. Actuators B* **120**, 305–312 (2006). <https://doi.org/10.1016/j.snb.2006.02.028>
7. F. Tokiwa, Electrostatic and electrokinetic potentials of surfactant micelles in aqueous solutions. *Adv. Colloid Interface Sci.* **3**(4), 389–424 (1972)
8. K. Bohinc et al., Incorporation of ion and solvent structure into mean-field modeling of the electric double layer. *Adv. Colloid Interface Sci.* **249**, 220–233 (2017)
9. M. Drab, V. Kralj-Iglic, Diffuse electric double layer in planar nanostructures due to Fermi–Dirac statistics. *Electrochim. Acta* **204**, 154–159 (2016)
10. D. Burgreen, F.R. Nakache, Electrokinetic flow in ultrafine capillary silts. *J. Phys. Chem.* **68**(5), 1084–1091 (1964)
11. M. Khan et al., Exact solution of an electroosmotic flow for generalized Burgers fluid in cylindrical domain. *Results Phys.* **6**, 933–939 (2016)
12. H. Ni, R.C. Amme, Ion redistribution in an electric double layer. *J. Colloid Interface Sci.* **260**, 344–348 (2003)
13. A. Jain, M.K. Jensen, Analytical modeling of electrokinetic effects on flow and heat transfer in microchannels. *Int. J. Heat Mass Transf.* **50**, 5161–5167 (2007)
14. G.D. Ngoma, F. Erchiqui, Heat flux and slip effects on liquid flow in a microchannel. *Int. J. Therm. Sci.* **46**, 1076–1083 (2007)
15. M. Shamshiri et al., Heat transfer and entropy generation analyses associated with mixed electrokinetically induced and pressure-driven power-law microflows. *Energy* **42**, 157–169 (2012)
16. Z. Wang, Y. Jian, Heat transport of electrokinetic flow in slit soft nanochannels. *Micromachines* **10**, 34 (2019)
17. V. Steffen et al., Debye-Huckel approximation for simplification of ions adsorption equilibrium model based on Poisson–Boltzmann equation. *Surf. Interfaces* **10**, 144–148 (2018)
18. C. Yang, D.Q. Li, Electrokinetic effects on pressure-driven liquid flows in rectangular microchannels. *J. Colloid Interface Sci.* **194**(1), 95–107 (1997)
19. S. Kandlikar et al., *Heat Transfer and Fluid Flow in Minichannels and Microchannels*, 1st edn. (Elsevier Ltd., Great Britain, 2006).
20. S. Yildirim, Exact and numerical solutions of Poisson equation for electrostatic potential problems. *Math. Probl. Eng.* **2008**, 1–11 (2008)
21. C. Wang et al., Characterization of electroosmotic flow in rectangular microchannels. *Int. J. Heat Mass Transf.* **50**, 3115–3121 (2007)
22. M. Manciu et al., On the surface tension and Zeta potential of electrolyte solutions. *Adv. Colloid Interface Sci.* **244**, 90–99 (2016)

Publisher's Note Springer Nature remains neutral with regard to jurisdictional claims in published maps and institutional affiliations.